RSC Advances

PAPER

View Article Online
View Journal | View Issue

Cite this: *RSC Adv.*, 2024, **14**, 7507

Advancements in sustainable platinum and palladium recovery: unveiling superior adsorption efficiency and selectivity with a novel silica-anchored acylthiourea adsorbent†

Malehlogonolo R. R. Mphahlele, [a] Alseno K. Mosai,[b] Hlanganani Tutu[a] and Izak A. Kotzé *[a]

This study addresses the pressing issue of depleting natural resources of platinum group metals (PGMs), driven by their widespread use in modern applications and increasing demand for renewable energy technologies. With conventional sources dwindling, the search for economically viable recovery methods from alternative sources has become crucial. Our focus was on innovating efficient recovery strategies, leading to the development of two novel silica-anchored adsorbents: DTMSP-BT-SG, a highly efficient acylthiourea adsorbent, and BTMSPA-SG, a silica-anchored amine adsorbent. We conducted comprehensive experiments under PGM mining wastewater conditions, varying parameters such as adsorbent mass, pH, concentration, contact time, competing ions, and volume. DTMSP-BT-SG demonstrated exceptional performance, achieving maximum adsorption efficiencies of >98% for Pt and >99% for Pd at pH 2, 0.5 g L^{-1} dosage, and 5 mg L^{-1} concentration. In contrast, under the same conditions, BTMSPA-SG recovered <56% and <89% of Pt and Pd, respectively. The experimental data for both adsorbents were analysed using Langmuir and Freundlich isotherm models for concentration and pseudo-first and second-order models for contact time. The Langmuir model best described the adsorption data, indicating homogenous monolayer adsorption of Pt and Pd. The kinetic models suggested a pseudo-second-order process, implying chemisorption. Furthermore, in the presence of competing ions and other PGMs, DTMSP-BT-SG exhibited significantly higher recovery rates for Pt and Pd compared to BTMSPA-SG. Overall, DTMSP-BT-SG emerged as a more selective and efficient adsorbent across varied parameters. Its exceptional adsorption efficiency, coupled with cost-effectiveness, positions it as a promising and competitive recovery agent for extracting PGMs from mining wastewaters.

Received 29th November 2023
Accepted 21st February 2024

DOI: 10.1039/d3ra08169a

rsc.li/rsc-advances

1. Introduction

PGMs have been widely used in catalysis, medical equipment, jewellery manufacturing, electronics *etc.*, due to their excellent physicochemical properties such as high catalytic activity, thermal stability, and corrosion resistance.[1–3] Termed also as the 'vitamin of the modern industry', these minerals play a critical role in the renewable energy revolution as they are essential active components in automotive vehicles and hydrogen fuel cells which both contribute to reducing greenhouse emissions.[2,4–6] Due to their contribution and advancement of the global economy, the consumption for PGMs is set to continue soaring, thus further intensifying their demand.[4,7,8] In 2023, the demand for PGMs especially, Pt and Pd was approximated to be 231.9 (Pt) and 305.8 (Pd) tonnes, whilst the supply (of combined primary and secondary sources) was 227.8 (Pt) and 304.5 (Pd) tonnes as reported by the Johnson Matthey PGM market report.[9] This data clearly indicates that the PGMs demand outstrips the supply. Moreover, it also highlights their scarcity which is attributed to their depleting natural resources, and complex processes of recovery.[3,4] Additionally, the high industrial usage of these metals will inevitably generate increased volumes of Pt- and Pd-containing wastewater.[2,5,8,10] Consequently, if discharged untreated, this industrial wastewater will not only cause environmental pollution (to soil and water resources) but, a sufficient amount of precious material will also be lost.[2,8,10] Therefore, the recovery of Pt and Pd from secondary sources such as refinery wastewater, holds the dual promise of

[a]*Molecular Sciences Institute, School of Chemistry, University of the Witwatersrand, Private Bag X3, WITS, Johannesburg, 2050, South Africa. E-mail: Izak.Kotze@wits.ac.za*

[b]*Department of Chemistry, Faculty of Natural and Agricultural Sciences, University of Pretoria, Lynnwood Road, Pretoria 0002, South Africa*

† Electronic supplementary information (ESI) available. See DOI: https://doi.org/10.1039/d3ra08169a

enriching these metals to benefitting industries, and also remediating pollution.[2,3,8,10]

Traditional and recent techniques that have been used for PGMs recovery from such solutions include solvent extraction, chemical precipitation, ion exchange, membrane separation, reverse osmosis, evaporation and adsorption.[10–14] However, some of these techniques have shortcomings such as poor selectivity, complex operational processes and low recovery rates.[10–14] Amongst the mentioned techniques, adsorption has emerged as the better option for metal recovery, owing to its cost-effectiveness, utilization of less energy and ability to significantly remove precious metals from aqueous solutions including those which are in very low concentrations.[8,10–14] Furthermore, adsorption displays several other advantages such as high removal efficiency, re-usability and tunability of the solid support by functionalizing it with organo-functional groups that will improve the selectivity of the adsorbent towards the metal of interest.[14–16] At present, a variety of adsorbents, especially those incorporating the amine functionality have been reported for PGMs recovery.[2,3,12,17] Amines are known for their high affinity and exceptional selectivity in recovering PGMs over other transition metals (Ni, Cu and Fe).[6,7,17] Hence, a lot of studies have focused on developing a multitude of amine-incorporated adsorbents such as chitosan, collagen fibre membranes, silica-based (poly)amine ion-exchangers, amino-functionalized magnetic sorbents, immobilized micro particles with ammonium centres and several other amide compounds for PGMs recovery.[2,3,14,17–21] Whilst amine adsorbents have been largely explored for their high PGM extraction abilities, very little has been documented on the use of acylthiourea-based adsorbents for PGMs recovery. Hence, this study sought out to develop a highly efficient and selective novel silica-anchored acylthiourea adsorbent that would potentially be used in Pt and Pd recovery from refinery solutions with low precious metal concentrations.

Acylthioureas are a ligand class known to have a pronounced affinity towards PGMs, especially under acidic chloride conditions.[22] These ligands contain multiple hard and soft donor atoms (O, N, S) that are available to bind to target metal ions.[22–25] Additionally acylthioureas are non-toxic, non-sensitive, odourless and can be readily prepared from cheap reagents in high yields through a facile two-step, one-pot synthetic procedure (Scheme 1).[22,23] To anchor the acylthiourea ligand, silica gel was chosen as an extraction support due to its large surface area, thermal and mechanical resistance, lack of swelling, hydrophilic properties, and a great resistance towards organic solvents.[26] Modifying the silica surface with the acylthiourea ligand will act to improve its efficiency, sensitivity, and selectivity in analytical applications, which is vital for a good adsorbent.[26–28] Furthermore, the covalent bond that forms between the ligand and the silica gel will prevent detachment during the adsorption studies thus allowing the adsorbent to be recycled and reused for further adsorption studies.[26]

This study aimed to develop an innovative, highly efficient and selective *N*,*N*-di(trimethoxysilylpropyl)-*N*′-benzoylthiourea modified silica gel (DTMSP-BT-SG) adsorbent. The adsorbent was prepared by functionalising silica gel with a novel acylthiourea ligand (*N*,*N*-di(trimethoxysilylpropyl)-*N*′-benzoylthiourea (DTMSP-BT)). The DTMSP-BT-SG adsorbent was used to recover Pt and Pd from aqueous solutions mimicking refinery wastewater. Parameters such as pH, adsorbent dosage, competing ions, initial concentration, volume *etc.*, were varied to obtain such solution conditions. Adsorption and kinetic isotherms were also studied to better understand the mechanisms and relationship of adsorption between the metal ions and the adsorbent. Moreover, the adsorption performance of DTMSP-BT-SG was tested against another amine-based adsorbent, bis(3-(trimethoxysilyl)propyl)amine modified silica gel (BTMSPA-SG), which was similarly prepared and used for Pt and Pd recovery under comparable conditions.

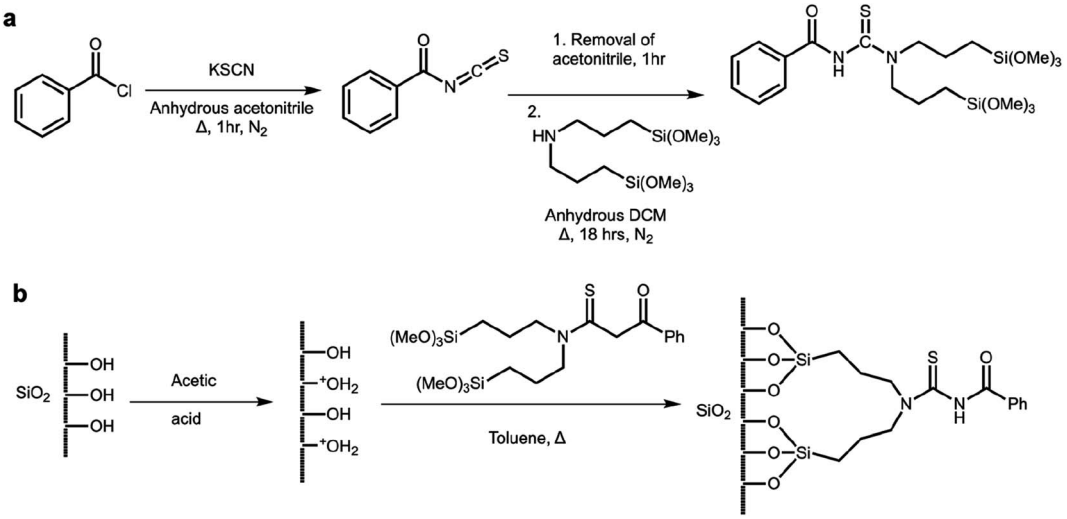

Scheme 1 Synthesis of DTMSP-BT and its immobilization onto silica gel.

2. Materials and methods

2.1. Chemicals and reagents

The synthetic reagents and analytical grade Pt and Pd standard solutions (1000 mg L^{-1} in 5% w/w of c(HCl)) were purchased from Sigma-Aldrich, South Africa. The Pt and Pd working solutions were made up from 100 mg L^{-1} stock solutions that were prior prepared and stored in the refrigerator at 4 °C. The pH of these solutions was adjusted with HCl and NaOH (0.01 mol L^{-1}).

2.2. Instrumentation

^{1}H and ^{13}C NMR spectra were recorded with Bruker Avance III 500 MHz (Germany). Mass Spectrometry was performed on a high-resolution Bruker Compact Q-TOF spectrometer (Germany). The functional groups of the ligand and adsorbents were determined using Fourier transform infrared spectroscopy (FT-IR) (Tensor 27, Bruker, Germany). Inductively coupled plasma optical emission spectroscopy (ICP-OES) (Spectro Genesis, Germany) was used for metal quantification. The surface morphology of the adsorbents was observed with scanning electron microscopy (SEM) (TESCAN Vega, Czech Republic). The chemical compositions and mineralogy were determined with X-ray fluorescence (XRF) (PAnalytical, Netherlands) and powder X-ray diffraction (PXRD) (D2-Phaser, Bruker, Germany) respectively. The surface area and pore characteristics of the adsorbents were determined using Brunauer–Emmet–Teller (BET) (TriStar 3000 V6.05 A, Micrometrics, USA) isotherms. Thermogravimetric analysis (TGA) and differential temperature analysis (DTA) (PerkinElmer Pyris 1 TGA, Massachusetts, USA) were used to determine the thermal stability of the adsorbents. Elemental analysis (varioELcube V4.0.13, Elementar, Germany) was used to quantify the C, H, N, and S elemental compositions of the adsorbents.

2.3. Synthesis of *N*,*N*-di(trimethoxysilylpropyl)-*N*′-benzoylthiourea (DTMSP-BT)

The synthetic procedure (Scheme 1a) described by Douglass and Dains was modified for preparation of DTMSP-BT.[25] Benzoyl chloride (1.2 mL/10 mmol) in dry acetonitrile (15 mL) was added into a solution of potassium thiocyanate (1 g/10 mmol) and anhydrous acetonitrile (20 mL). The reaction mixture was refluxed for 1 h at 80 °C to yield an intermediate that was cooled down and placed under vacuum to remove the acetonitrile. Anhydrous dichloromethane (DCM) (20 mL) was added to the isolated intermediate followed by the addition of bis(3-(trimethoxysilyl)propyl)amine (BTMSPA) (3.12 mL/9.5 mmol) in DCM (20 mL). The reaction mixture was stirred overnight at 40 °C and the resultant product was cooled to room temperature and filtered. The DCM of the filtrate was removed under reduced pressure and the product was obtained as an orange viscous liquid. Yield: 74%. ^{1}H NMR (500 MHz, $CDCl_3$), δ(ppm): 8.29 (s, 1H: N–H), 7.82 (d, $J = 3.0$, 3.0 Hz, 2H, H^{e}, H^{f}), 7.56 (t, $J = 6.0$ Hz, 1H, H^{i}), 7.46 (t, $J = 6.0$, 6.0 Hz, 2H, H^{g}, H^{h}), 3.94 (t, $J = 6.0$ Hz, 2H, H^{d}), 3.50–3.57 (m, 20H: (t, $J = 6.0$ Hz, 2H, Hd′), (s, 9H, H^{a}), (s, 9H, $H^{a'}$)), 1.92 (q, $J = 6.0$ Hz, 2H, H^{c}), 1.77 (q, $J = 6.0$ Hz, 2H, Hc′), 0.74 (t, $J = 6.0$ Hz, 2H, H^{b}), 0.52 (t, $J = 6.0$ Hz, 2H, $H^{b'}$). ^{13}C NMR (500 MHz) ($CDCl_3$), δ(ppm): 180.18 (C═S), 163.57 (C═O), 133.10 (C^{5}), 132.72 (C^{10}), 128.25 (C^{8}, C^{9}), 127.81 (C^{6}, C^{7}), 55.58 (C^{4}), 55.53 ($C^{4'}$), 51.40 (C^{1}), 54.40 ($C^{1'}$), 21.45 ($C^{3'}$), 19.59 (C^{3}), 6.23 (C^{2}), 6.21 ($C^{2'}$). FT-IR: ν (cm^{-1}): 3256 (N–H), 2942, 2840 (C–H), 1685 (C═O), 1071 (Si–O–Si). ESI-MS (m/z): calc. 504.18 [M], exp. 505.21 $[M + H]^{+}$.

2.4. Immobilization of DTMSP-BT and BTMSPA onto silica gel

The procedure (Scheme 1b) reported by Erdem *et al.*, was used to functionalize the silica gel (Davisil Grade 710, pore size 50–76 Å) with DTMSP-BT and BTMSPA.[29]

Silica gel (0.50 g) and 0.01 M acetic acid (20 mL) were mixed for 10 min to activate the silanol groups. The mixture was filtered using suction and washed with distilled water before being added to a solution of toluene (20 mL) and DTMSP-BT (0.30 mL). The reaction mixture was refluxed for 20 h at 110 °C, and thereafter, cooled and filtered. The obtained functionalized silica particles were washed with toluene and dried at 80 °C for 8 h. The immobilization of BTMSPA onto the silica was carried out in a similar manner (Scheme S1, ESI†).

2.5. Batch adsorption studies

Batch adsorption experiments (Fig. S1, ESI†) were carried out to determine the effect of adsorbent dosage (5–50 mg), pH (2–9), concentration (0.5–50 mg L^{-1}), contact time (10–1440 min), volume (20–50 mL), and competing ions (Fe, Co, Ni, Ca, Mg, K, Zn) on the recovery of Pt and Pd by DTMSP-BT-SG and BTMSPA-SG. To perform the experiments, 20 mL of the metal solutions and the relevant adsorbent mass were added into centrifuge tubes (50 mL). The tubes were placed on an elliptical benchtop shaker (Labcon, South Africa) to agitate (150 rpm) at room temperature (25 °C) until equilibrium (optimised time, 4 h). The contents were centrifuged (50 rpm, 25 °C) for five minutes and filtered using 0.45 μm Whatman filter paper (Whatman™, UK). The filtrate was analysed with ICP-OES to determine the residual metal concentration.

The amount of metal adsorbed per unit mass, q_e (mg g^{-1}) and the adsorption efficiency (%) were calculated with eqn (1) and (2) respectively. The efficiency of the adsorbents in adsorbing Pt and Pd was assessed by performing the batch adsorption experiments in duplicates ($n = 2$).

$$q_e = \left(\frac{(C_0 - C_e)V}{m}\right) \quad (1)$$

$$\text{Adsorption efficiciency} = \frac{(C_0 - C_e)}{C_0} \times 100\% \quad (2)$$

C_0 and C_e (mg L^{-1}), are the initial and equilibrium metal concentrations respectively, V (L) is the solution volume, and m (g) is the adsorbent mass.

3. Results and discussion

3.1. Characterization of DTMSP-BT

The molecular structure and successful synthesis of DTMSP-BT were well confirmed by one- and two-dimensional NMR spectroscopy, FT-IR Spectroscopy, and mass spectrometry. The ^{1}H

NMR spectrum (Fig. S2†) displayed the deshielded N–H proton as a broad singlet at 8.29 ppm. Three signals (H^e/H^f, H^g/H^h and H^i) corresponding to the five protons of the benzene ring were observed in the aromatic region (7.46–7.82 ppm). The deshielded doublet at 7.81 ppm corresponded to the H^e and H^f that are adjacent to the electron-withdrawing carbonyl substituent.

The aliphatic protons of the trimethoxysilylpropyl substituents on the nitrogen occurred in different chemical environments due to delocalization of electrons around the thioamidic moiety.[30] This effect causes a partial double bond character around the thioamidic bond which restricts rotation, and resultingly the aliphatic protons are inequivalent.[30] The H^d/$H^{d'}$ (3.94 ppm) protons were the most deshielded due to the nitrogen. The second H^d/$H^{d'}$ signal is obscured by the two singlets around 3.50 ppm, and it is clearly distinguished on the COSY (Fig. S3†) and HSQC (Fig. S4†) spectra. The sharp singlets at 3.50 and 3.57 ppm corresponded to the H^a/$H^{a'}$ protons. Lastly, the quintets (1.77–1.92 ppm) and triplets (0.74–0.52 ppm) were assigned to H^c/$H^{c'}$ and H^b/$H^{b'}$ respectively.

The ^{13}C spectrum (Fig. S5†) revealed the thiocarbonyl (C=S) and carbonyl (C=O) carbons to be the most deshielded signals at 180.18 and 163.57 ppm respectively. C=S was distinguished from the C=O on HMBC (Fig. S6†) where H^d and $H^{d'}$ coupled to the C=S carbon through long-range coupling. The aromatic (C^{10}, C^9, C^8, C^7, C^6) and aliphatic carbons ($C^{4'}$/C^4, $C^{3'}$/C^3, $C^{2'}$/C^2, $C^{1'}$/C^1) were all assigned using HSQC for C–H correlation as well as ^{13}C DEPT (Fig. S7†). The quaternary carbon at 132.70 ppm was assigned to C^5.

The FT-IR spectrum (Fig. S8†) revealed the C=O stretch of DTMSP-BT at 1685 cm^{-1}. The C=S stretch of acylthioureas usually occurs around 800–1500 cm^{-1}, thus its presence can be assumed.[22–24] The N–H (3256 cm^{-1}) and Si–O–Si (1071 cm^{-1}) stretches further confirmed the ligand structure.[31] Mass spectrometry (Fig. S9†) also confirmed the identity of the ligand as the predicted isotopologue pattern of the ligand agreed with the experimentally obtained spectrum. The ESI-MS $[M + H]^+$ of 505.21 *m*/*z* was observed and it correlated with the calculated value of [M] 504.18 *m*/*z*.

3.2. Characterization of the adsorbents

The successful functionalization of the silica gel with the acylthiourea ligand and the amine reagent was confirmed with ^{13}C solid-state NMR spectroscopy, FT-IR spectroscopy, and CHNS elemental analysis. Other techniques used for further characterization of the adsorbents include Scanning Electron Microscopy (SEM), X-ray fluorescence (XRF), Powder X-ray diffraction (PXRD), Brunauer–Emmett–Teller (BET) surface area analysis, thermogravimetric analysis (TGA) and differential temperature analysis (DTA).

FT-IR confirmed the successful immobilization of DTMSP-BT and the amine reagent onto the silica gel, as all the expected peaks were observed on the spectra. The superimposed FT-IR spectra (Fig. S10†) of the silica gel, DTMSP-BT, and DTMSP-BT-SG, indicated a characteristic peak at 1688 cm^{-1} corresponding to the C=O stretch of DTMSP-BT.[22,30] The peaks at 3261 and 2943 (2841) cm^{-1} were assigned to the N–H and C–H stretches of the DTMSP-BT ligand.[30] Additionally, the silica gel is frequently distinguished by the broad stretch of the siloxane group (Si–O/Si–O–Si) observed around 1100 cm^{-1}.[29,31] This siloxane group has been reported to have a very strong infrared absorption, which results in the band covering the regions from 1000–1200 cm^{-1}.[29,31,32] Moreover, this band also prevents the observation of the other functional groups of the ligand found in this region.[31] Additional stretches of the silica gel can be observed at 1649 and 3464 cm^{-1}.[31–33] These are usually attributed to the bending vibrations of physically adsorbed H_2O molecules and OH vibrations respectively which are caused by the hydrogen-bonded surface silanol groups of the silica gel.[31–33] The FT-IR spectra of the BTMSPA-SG adsorbent (Fig. S11†) also confirmed functionalization of the amine reagent onto the silica gel. This was marked by the appearance of the peaks at 3464 and 2940 cm^{-1} which corresponded to the N–H and C–H groups. Similarly, to DTMSP-BT-SG, the strong silica Si–O–Si stretch at 1085 cm^{-1} further proved that the amine was bound to the silica gel.

The successful addition of the amine and DTMSP-BT onto silica gel was also confirmed by the ^{13}C solid-state NMR spectra in Fig. 1. The assignment of the amine (BTMSPA-SG) spectrum (Fig. 1a) was easily achieved using previous literature.[17,34] C^4 occurred downfield at 50 ppm due to deshielding by the adjacent electronegative nitrogen. The two signals occurring at 20 and 10 ppm were assigned to C^3 and C^2 respectively. The electropositive silicon atom adjacent to C^2 shields it, hence, C^2 occurred at a lower chemical shift.

The assignment of the aliphatic protons in the DTMSP-BT-SG spectrum (Fig. 1b) was achieved in a similar manner to the amine. Interestingly, it can also be noted that the C^4 signal of DTMSP-BT-SG in the solid-state NMR spectrum is broader than the C^2 and C^3 signals. This broadness can be speculated to be due to the presence of some residual methoxy groups that were not immobilized, and these can be observed as the C^1 and $C^{1'}$ peaks in the ^{13}C solution NMR. This was also corroborated by a study done by Kramer *et al.* that reported the immobilization of polyamines onto silica gel.[9,34] Their solid-state results indicated that some of the $Si(OCH)_3$ groups that don't react with the silica will remain present after immobilization, hence they'll be observed as residual signals in the spectrum.[9,34]

To assign the remaining signals that are not present in the amine-functionalized silica, the ^{13}C solid-state NMR of the silica-anchored acylthiourea adsorbent was compared to that of the ^{13}C solution NMR of the ligand (Fig. 1c) to note the appearance of the added functional groups from the free ligand. The aromatic carbons were observed around 125.48 ppm whilst the C=S and C=O groups were found at 178.29 and 163.39 ppm respectively. The resemblance of the ^{13}C solution NMR of the free ligand to that of the ^{13}C solid state of the adsorbent, fully confirmed that the ligand was successfully immobilized onto the silica.

The SEM images (Fig. S12†) indicated that all the adsorbents had a non-uniform surface with varying particle sizes and shapes.[33,35] The particles were also observed to be unevenly distributed on the adsorbents' surfaces.[29,35] The P-XRD patterns (Fig. S13a†) of the adsorbents all showed a dominant peak at

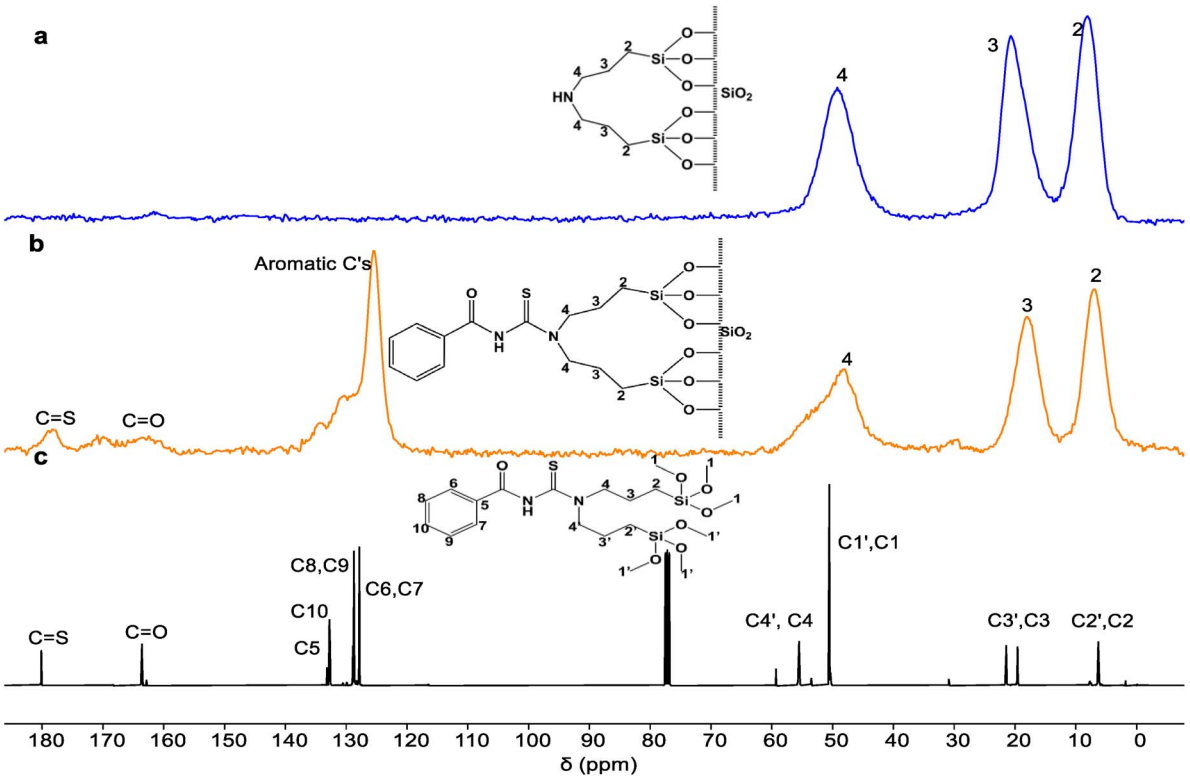

Fig. 1 The ^{13}C solid state NMR spectrum of (a) BTMSPA-SG, (b) DTMSP-BT-SG stacked with the ^{13}C solution NMR spectrum of (c) the free ligand (DTMSP-BT).

around $2\theta = 21.9°$ which is indicative of amorphous materials.[35] Additionally, the modification of the silica gel with BTMSPA and DTMSP-BT didn't contribute to any structural changes on the silica.[36] This is usually attributed to the high chemical stability of the silica gel.[36,37] The type IV BET isotherms in Fig. S13b† indicate N_2 adsorption taking place in two stages.[37] The first stage at low pressures describes monolayer N_2 adsorption and filling of the micropores, whilst the second stage at higher pressures, indicates filling of the mesopores and formation of multilayers.[36,37] The isotherms indicated that after the immobilization, the amount of N_2 adsorbed decreases due to partial filling of the silica pores, as well as its surface occupancy with the DTMSP-BT and BTMSPA groups.[29] This is also noted from the low surface area and decreased pore volume obtained after the modification process (Table S1†).[36]

The TGA and DTA results (Fig. S14†) indicated that there was an initial 3–5% weight loss for all the adsorbents around 40–100 °C, which can be attributed to the removal of adsorbed water molecules.[29,37] Beyond 100 °C, there was a further percentage weight loss, which is due to loss of the functional groups from the adsorbents' surfaces.[29,37] DTMSP-BT-SG and BTMSPA-SG recorded a higher total % weight loss than the silica which denotes the extra functionality present on the adsorbents.[37] The XRF chemical compositions (Table S2†) indicated that the silica and the adsorbents were dominantly composed of SiO_2. The reduced SiO_2 content observed for DTMSP-BT-SG and BTMSPA-SG is due interaction of the SiO_2 molecules of the silica with DTMSP-BT and BTMSPA to form the Si–O–Si moiety which binds these groups to the silica surface.[31]

3.2.1 Elemental analysis and ligand loading. The CHNS analysis (Table S3†) also indicated that there was a high carbon percentage for all the adsorbents which is a result of their propyl chains as well as the carbons of the benzoyl group on DTMSP-BT-SG. To quantify the amount of ligand present on the silica surface, the carbon and nitrogen elemental data were used to calculate the ligand concentrations reported in Table S3.† The method used for the calculations is outlined below (Calculation 1) using the DTMSP-BT-SG elemental data. The obtained nitrogen ligand concentrations were 1.03 and 1.68 mmol g^{-1} for DTMSP-BT-SG and BTMSPA-SG respectively, and these were used to account for the observed Pt and Pd adsorption capacities of the adsorbents.

3.2.1.1 Calculation 1: ligand concentrations. The assumption that all the alkoxy substituents were immobilized was made thus, the chemical composition of the ligand on silica is $C_{14}H_{21}N_2OSSi_2$.

Based on nitrogen content:

$$n = \frac{m}{M}$$

n (mol) is the number of moles, m (g) is the elemental mass and M (g mol^{-1}) is the molar mass of the element.

$$n = \frac{2.89\ \text{g}}{2 \times 14.01\ \text{g mol}^{-1}} \times 1000 = 103.14\ \text{mmol}$$

$$\text{ligand/100 g silica} = \frac{103.14\ \text{mmol}}{100\ \text{g}} = 1.03\ \text{mmol g}^{-1}$$

Based on carbon content:

$$n = \frac{18.02\ \text{g}}{14 \times 12.011\ \text{g mol}^{-1}} \times 1000 = 107.16\ \text{mmol}$$

$$\text{ligand/100 g silica} = \frac{107.16\ \text{mmol}}{100\ \text{g}} = 1.07\ \text{mmol g}^{-1}$$

3.3. Batch adsorption studies

3.3.1. Effect of adsorbent dosage. The effect of mass (Fig. 2a) indicated that the Pt and Pd adsorption increased with adsorbent mass, because of the high number of active sites available.[38,39] DTMSP-BT-SG significantly recovered both Pt (>98%) and Pd (>95%) at all the studied dosages whilst, BTMSPA-SG only recovered Pd (>89%) better than Pt. The high removal efficiency of DTMSP-BT-SG in comparison to BTMSPA-SG can be attributed to the high acylthiourea affinity towards PGMs which has been reported to be favored in acidic conditions.[30,40] Additionally, the high Pt and Pd removal by this adsorbent was substantiated by the adsorbent-to-metal ratios (Table S4†) which were calculated from the elemental analysis data. The determined ratios of DTMSP-BT-SG to Pt (4.15) and Pd (3.69), were observed to be less than those of BTMSPA-SG to Pt (49.36) and Pd (14.24), thus signifying the great adsorption capacity of DTMSP-BT-SG as only a small amount would be required to remove both metals.[41,42] The optimum dosage for both metal ions was 0.5 and 1.0 g L^{-1} for DTMSP-BT-SG and BTMSPA-SG respectively.

3.3.2. Effect of pH. The effect of pH results (Fig. 2b) illustrated that the removal efficiency decreased with increasing pH, especially for BTMSPA-SG as the adsorption dropped to 72% for Pd and 5% for Pt, whilst that of DTMSP-BT-SG remained high. The maximum Pt and Pd adsorption efficiency by both adsorbents was observed at pH 2 and this can be attributed to the favourable adsorption of the stable Pt and Pd chloro-complexes ($[PtCl_6]^{2-}$, $[PtCl_4]^{2-}$ and $[PdCl_4]^{2-}$) which form in highly acidic chloride concentrations.[32,34,43] These species can get adsorbed through various mechanisms of adsorption including: ion-pairing, ion exchange, and complexation.[36,37] However, at low pHs the ion-pairing mechanism takes precedence due to protonation of the surface donor atoms which contribute to positively charged adsorbent surfaces that attract the negative species.[17,42,44]

At high pHs, the Pt and Pd chloro species get aquated to form a diverse number of species ($[PtCl_5(H_2O)]^-$, $[PtCl_4(H_2O)_2]$, $[PdCl_3(H_2O)]^-$, $[PdCl_2(H_2O)_2]$) which are not prone to separation.[9,42,44] However, if adsorption does take place, it will be through the coordination mechanism as the surface functional groups no longer get protonated but rather, coordinate to metal ions through their lone pairs.[34,45] At these conditions (pH > 4), the Pt and Pd recovery by DTMSP-BT-SG remained significant (>98%), but decreased for BTMSPA-SG. This indicates that the present species were favoured for adsorption by DTMSP-BT-SG, where coordination can be deduced to occur through the O, N, and S donor atoms of this adsorbent, which are absent on BTMSPA-SG. Adsorption through coordination occurs according to the Pearson hard/soft acid/base (HSAB) theory, where a soft metal ion such as Pd(II) will have a high affinity for sulphur (a soft donor atom).[34,36] The ability of DTMSP-BT-SG to recover considerable amounts of Pt and Pd in both the acidic and basic pH mediums, deems it a better candidate over BTMSPA-SG, for precious metals recovery.

3.3.3. Effect of concentration and volume. The effect of concentration (Fig. 3a) indicated that the adsorbed amount of Pt and Pd by DTMSP-BT-SG increased with concentration from 2–10 mg L^{-1}, and thereafter decreased to 50 mg L^{-1}. The initial increase in recovery can be attributed to the availability of active sites owing to the low metal concentration.[37] However, increasing the concentration leads to a maximum occupancy on the adsorbent sites, beyond which the efficiency will start decreasing.[37] The Pt and Pd removal efficiency by BTMSPA-SG started decreasing after 2 mg L^{-1} and was more significant due to the low surface area and adsorption capacity of this adsorbent.[37] The results further revealed that DTMSP-BT-SG outperforms BTMSPA-SG, as it recorded a high Pt and Pd uptake of >95%, whilst BTMSPA-SG only recovered Pd (92%) better than Pt (48%).

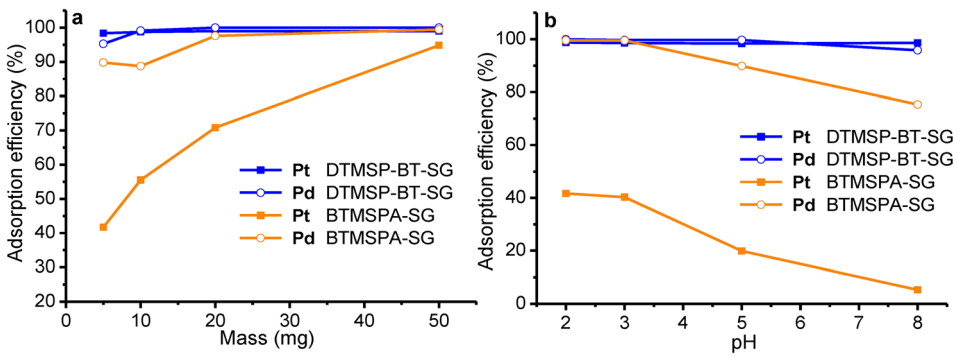

Fig. 2 Effect of (a) adsorbent dosage (5–50 mg) and (b) pH (2–9) on the recovery of Pt and Pd (mass = 10 mg, pH = 2, concentration = 5 mg L^{-1}, time = 4 h, temp = 25 °C, vol. = 20 mL, n = 2, RSD < 3%).

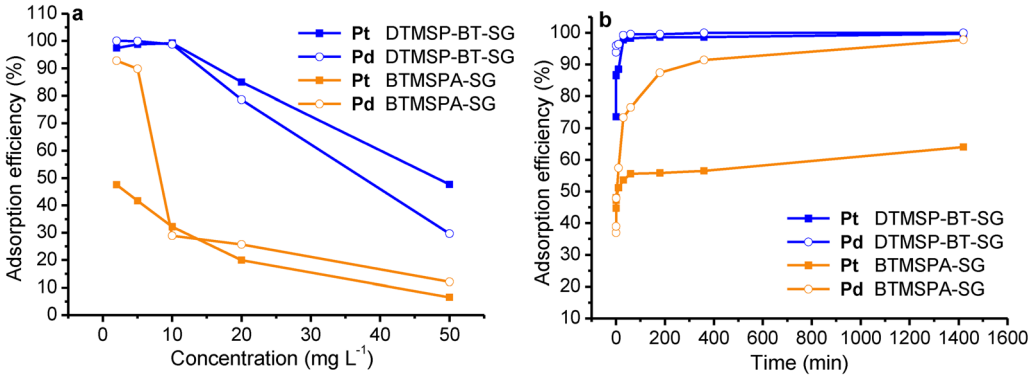

Fig. 3 Effect of (a) concentration (2–50 mg L^{-1}) and (b) contact time (0.17–1440 min) on the recovery of Pt and Pd (mass = 10 mg, concentration = 5 mg L^{-1}, pH = 2, time = 4 h, temp = 25 °C, vol = 20 mL, n = 2, RSD < 3%).

The effect of volume (20–50 mL) (Fig. S15†) further illustrated that DTMSP-BT-SG had a higher adsorption capacity than BTMSPA-SG as it captured more Pt and Pd with increasing solution volume.[46,47] The low adsorption capacity of BTMSPA-SG results in its fast saturation which is observed on the efficiency graph (Fig. S15a†), where the Pt and Pd adsorption decreased rapidly with volume, whilst that of DTMSP-BT-SG remained relatively high (>95%) throughout.[46,47] Additionally, the Langmuir q_m values were used to determine the volumes at which maximum adsorption was expected (Table S4†). The results indicated that Pt and Pd adsorption by BTMSPA-SG will start decreasing after volumes of 13.26 and 25.06 mL respectively, whilst for DTMSP-BT-SG, adsorption will only decrease after 97.04 (Pt) and 59.36 (Pd) mL. This further signifies the superiority of DTMSP-BT-SG over BTMSPA-SG as it recovered significant amounts of Pt and Pd in large solution volumes, which is vital in refineries where higher volumes of waste solutions are realeased.[14,48]

3.3.3.1 Adsorption isotherms. The adsorption equilibrium data were fitted with the Langmuir and Freundlich isotherms.[48,49] These models provide information about the adsorption mechanisms, the adsorbent's surface properties, and their affinities towards metal ions.[48–50] The Langmuir isotherm (eqn (3)) assumes monolayer adsorption onto a homogenous adsorbent surface with a finite number of sites that have identical energies and are equally available for adsorption.[13,51,52] The Freundlich (eqn (4)) assumes adsorption onto a heterogenous surface with active sites that are unequal and have different energies.[49,53]

$$\frac{C_e}{q_e} = \left(\frac{1}{q_m}\right) C_e + \left(\frac{1}{K_L q_m}\right) \quad (3)$$

$$q_e = K_f C_e^{\frac{1}{n}} \quad (4)$$

q_m (mg g^{-1}) is the maximum monolayer coverage, K_L (L mol^{-1}) is the Langmuir constant, K_f ((mg g^{-1}) ((mol $L^{-1})^{1/n})^{-1}$) is the Freundlich constant, and n is the adsorption intensity.

The adsorption models (Table S5†) indicated that the Langmuir best described the experimental data (R^2 > 0.99), therefore monolayer adsorption took place.[13–15] The Pt and Pd q_m values were greater for DTMSP-BT-SG than BTMSPA-SG, highlighting their favourable adsorption by the former adsorbent. The value of K_L which quantitatively reflects the affinity of the adsorbents towards metal ions was higher for Pd for both DTMSP-BT-SG and BTMSPA-SG thus confirming its high adsorption which was observed throughout.[40] However, for Pt, K_L was greater for DTMSP-BT-SG thus, suggesting that this adsorbent is better suited to be employed in refinery wastewater remediation as it recovers both metals efficiently.[40]

The q_m of DTMSP-BT-SG and BTMSPA-SG was further compared to other widely known adsorbents used for Pt and Pd recovery (Table S6†). The q_m values of DTMSP-BT-SG were comparable to some of the adsorbents, thus implying that DTMSP-BT-SG has a remarkable adsorption capacity with various active sites available to extract a high quantity of metals.[10] Additionally, when compared to the amine adsorbent (BTMSPA-SG) in this study, DTMSP-BT-SG fared better, thus making it a high-performing adsorbent with potential to be used for PGMs recovery by industries that utilize these metals.[10,48]

3.3.4 Effect of contact time. The contact time studies (Fig. 3b) revealed that there was a rapid adsorption of Pt and Pd by DTMSP-BT-SG within the first 60 min. This is indicative of the high number of active sites that are readily available at the start of the adsorption process.[51] Equilibrium was reached beyond this point as marked by the constant adsorption efficiency.[15,52] For BTMSPA-SG, equilibrium adsorption of Pt and Pd was only observed after 3 h, thus indicating slower adsorption by this adsorbent. Additionally, the adsorption efficiency of both metals was higher for DTMSP-BT-SG than BTMSPA-SG, which can be attributed to its high surface area hence, making it more economical to use.

3.3.4.1 Kinetic models. Kinetic models deduced from the contact time data can aid in understanding the adsorption mechanisms.[49,50] The pseudo-first-order model (eqn (5)) assumes physical adsorption through weak van der Waals forces.[13,52] The pseudo-second-order model (eqn (6)) describes the adsorption process to be largely controlled by chemisorption.[53,54]

$$\log(q_e - q_t) = \log q_e - \frac{k_1 t}{2.303} \quad (5)$$

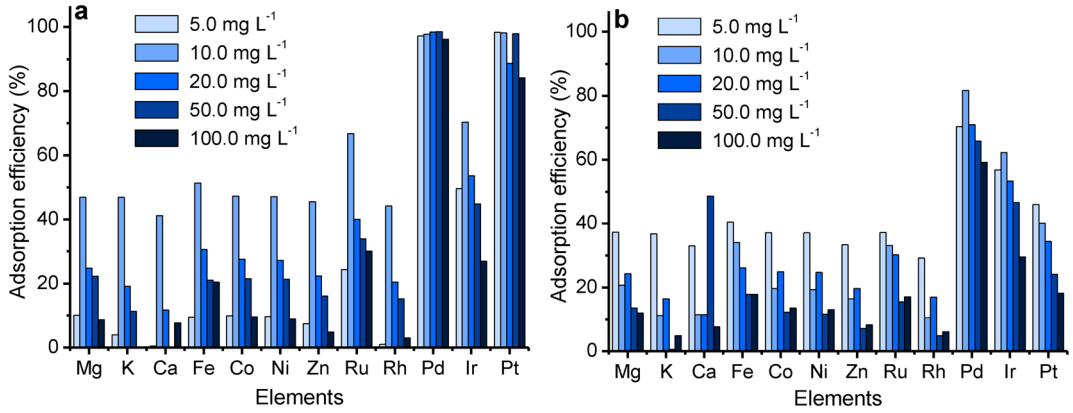

Fig. 4 Effect of competing ions on the recovery of Pt and Pd by (a) DTMSP-BT-SG and (b) BTMSPA-SG (mass = 10 mg, pH = 2, concentration = 5 mg L^{-1}, temp. = 25 °C, time = 4 h, vol. = 20 mL, n = 2, RSD < 3%).

$$\frac{t}{q_t} = \frac{1}{k_2 q_e^{\,2}} + \frac{1}{q_e} t \quad (6)$$

q_t (mg g^{-1}) is the adsorption capacity at time t, k_1 (min^{-1}) and k_2 (g mg^{-1} min^{-1}) are the pseudo-first and second-order rate constants respectively.

The results (Table S7†) indicated that the pseudo-second-order model best described the adsorption data (R^2 > 0.99) therefore, chemical adsorption took place.[13,54] The closeness of the calculated adsorption capacity ($q_{e(calc)}$) to the experimentally determined adsorption capacity ($q_{(exp)}$) was used to further validate the mechanism of adsorption.[13] The obtained $q_{e(exp)}$ values for both metals and adsorbents were similar to the $q_{e(calc)}$ values of the pseudo-second-order model, thus validating the chemisorption mechanism.[13,15]

The Pt and Pd k_2 values for DTMSP-BT-SG were more than ten times higher than those observed for BTMSPA-SG, which further confirms their fast and favourable adsorption by DTMSP-BT-SG.[42] Since the pseudo-second-order model assumes that the functional groups on the adsorbents' surfaces are responsible for metal uptake, this substantiates the high Pt and Pd recovery by DTMSP-BT-SG which contains more donor groups than BTMSPA-SG.[40,42,53]

3.3.5. Effect of competing ions. The selectivity of both adsorbents towards Pt and Pd was investigated by performing adsorption studies in the presence of competing metal ions (Fe, Co, Ni, Ca, Mg, K, Zn).[52] The PGMs concentration was kept at 5 mg L^{-1} whilst that of the ions was varied from 5–100 mg L^{-1}. The results (Fig. 4a) indicated that the Pt and Pd uptake by DTMSP-BT-SG was not negatively affected by the presence of other ions instead, their uptake increased for some concentrations, which may be a result of adsorbent-Fe-analyte synergistic effect.[13,15] Moreover, DTMSP-BT-SG was selective for Pt and Pd, as evidenced by the recovery efficiencies. BTMSPA-SG (Fig. 4b) displayed a high recovery for Pd (82%) over Pt (<50%) in the presence of ions. DTMSP-BT-SG further proved to be more efficient over BTMSPA-SG, as it selectively recovered significant amounts of both Pt and Pd even at elevated concentrations of competing ions, thus it can be used in PGMs refineries containing these ions.

4. Conclusion

This work illustrated the facile synthesis of novel DTMSP-BT ligand, and its immobilization onto silica gel to afford a highly efficient DTMSP-BT-SG adsorbent which was utilized for Pt and Pd recovery. The extraction capabilities of DTMSP-BT-SG were compared against an amine (BTMSPA-SG) adsorbent that was similarly prepared. NMR, FT-IR, elemental analysis, BET, and several other characterization techniques confirmed the identity of the ligand and adsorbents. The adsorption experiments indicated that at the optimal conditions (dosage of 0.5 g L^{-1}, a concentration of 5 mg L^{-1} and a solution pH 2), DTMSP-BT-SG displayed a higher Pt (98%) and Pd (>99%) recovery than BTMSPA-SG (Pt (56%) and Pd (89%)). The superiority in Pt and Pd recovery by DTMSP-BT-SG was attributed to its higher adsorption capacity (>29.68 mg g^{-1}) when compared to BTMSPA-SG (<12.53 mg g^{-1}).

In addition to outperforming the amine adsorbent (BTMSPA-SG) in Pt and Pd recovery, DTMSP-BT-SG displayed other significant attributes in the adsorption studies. These included the ability to efficiently recover both metals across the acidic and basic pH ranges, the capacity to adsorb elevated amounts of Pt and Pd in low metal concentration solutions and being able to maintain an enhanced selectivity for Pt and Pd even in the presence of competing ions. Coupled with its ease of preparation, operation and cost-effectiveness, these factors make DTMSP-BT-SG a suitable adsorbent and promising alternative to be applied in refinery wastewater for precious metal recovery. The introduction of DTMSP-BT-SG will contribute significantly to the enrichment of these metals to the global economy and simultaneously play an active role in pollution mitigation. Moreover, the optimal conditions established in this work will set a benchmark for conducting column-based adsorption experiments in future studies, which will aid in assessing the practical applicability of the adsorbents on a large industrial scale.

Conflicts of interest

The authors declare no conflict of interest.

Acknowledgements

The authors thank the National Research Foundation (NRF) for financial support and the University of the Witwatersrand for the research facilities.

References

1 T. Bossi and J. Gediga, *Johnson Matthey Technol. Rev.*, 2017, **61**, 111–121.
2 L. Zhao, X. Ma, J. Xiong, Q. Zhou, W. Chen, Z. Yang, F. Jiang, S. Wang, X. Yang and H. Bai, *J. Environ. Chem. Eng.*, 2023, **11**, 110549.
3 T. Ge, X. Zhou, L. Xu, Y. Sun, C. Yang, Y. Tian and Z. Zhao, *Miner. Eng.*, 2024, **206**, 108504.
4 W. Wang, Q. Tan, J. F. Chiang and J. Li, *Front. Environ. Sci. Eng.*, 2017, **11**, 1.
5 A. Haleem, F. Wu, W. Wang, M. Ullah, H. Li, A. Shah and J. Pan, *Sep. Purif. Technol.*, 2024, **331**, 125500.
6 R. Gao, X. Wang, X. Zhang, S. Zhang, X. Li, X.-F. Yu and L. Bai, *Sep. Purif. Technol.*, 2023, **316**, 123771.
7 W. Xu, F. Wang, S. Chen, K. Zhang and K. Tang, *Sep. Purif. Technol.*, 2024, **328**, 125039.
8 T. C. Maponya, K. Makgopa, T. R. Somo, D. M. Tshwane and K. D. Modibane, *Environ. Nanotechnol., Monit. Manage.*, 2023, **20**, 100805.
9 Johnson Matthey PGM Market Report May 2023, **https://matthey.com/products-and-markets/pgms-and-circularity/pgm-markets/pgm-market-reports**, accessed 16 January 2024.
10 A. Haleem, F. Wu, M. Ullah, T. Saeed, H. Li and J. Pan, *Sep. Purif. Technol.*, 2024, **329**, 125213.
11 M. K. Jha, D. Gupta, J. Lee, V. Kumar and J. Jeong, *Hydrometallurgy*, 2014, **142**, 60–69.
12 I. Yakoumis, M. Panou, A. M. Moschovi and D. Panias, *Clean. Eng. Technol.*, 2021, **3**, 100112.
13 A. K. Mosai and H. Tutu, *J. Dispersion Sci. Technol.*, 2020, **43**, 1016–1027.
14 A. N. Nikoloski, K. L. Ang and D. Li, *Hydrometallurgy*, 2015, **152**, 20–32.
15 A. K. Mosai, *Miner. Eng.*, 2021, **163**, 106770.
16 P. Jal, *Talanta*, 2004, **62**, 1005–1028.
17 J. Kramer, W. L. Driessen, K. R. Koch and J. Reedijk, *Hydrometallurgy*, 2002, **64**, 59–68.
18 W. Yoshida, Y. Baba, F. Kubota, N. Kamiya and M. Goto, *J. Chem. Eng. Jpn.*, 2017, **50**, 521–526.
19 O. E. Fayemi, A. S. Ogunlaja, E. Antunes, T. Nyokong and Z. R. Tshentu, *Sep. Sci. Technol.*, 2014, **50**, 1497–1506.
20 Y. Geng, J. Li, W. Lu, N. Wang, Z. Xiang and Y. Yang, *Chem. Eng. J.*, 2020, **381**, 122627.
21 K. Matsumoto, Y. Sezaki, S. Yamakawa, Y. Hata and M. Jikei, *Metals*, 2020, **10**, 324.
22 H. A. Nkabyo, I. Barnard, K. R. Koch and R. C. Luckay, *Coord. Chem. Rev.*, 2021, **427**, 213588.
23 M. Shoaib, M. Ayaz, M. Tahir and S. Shah, *J. Chem. Soc. Pak.*, 2016, **28**, 479–486.
24 A. Saeed, R. Qamar, T. A. Fattah, U. Flörke and M. F. Erben, *Intermediat*, 2016, **43**, 3053–3093.
25 I. B. Douglass and F. B. Dains, *J. Am. Chem. Soc.*, 1934, **56**, 1408–1409.
26 P. Jal, *Talanta*, 2004, **62**, 1005–1028.
27 K. N. Barquist, PhD thesis, University of Iowa, 2009, DOI: **10.17077/etd.xztd7s2g**.
28 T. A. Hamza, A. H. Sherif and E. A. Abdalla, *Stomatological Dis. Sci.*, 2007, **1**, 3–7.
29 A. Erdem, T. Shahwan, A. Çağır and A. E. Eroğlu, *Chem. Eng. J.*, 2011, **174**, 76–85.
30 T. Peega, R. N. Magwaza, L. Harmse and I. A. Kotzé, *Dalton Trans.*, 2022, **50**, 11742–11762.
31 P. Launer, Infrared analysis of organosilicon compounds, in *Silicon Compounds: Silanes & Silicones*, ed. B. Arkles, Gelest Inc, Morrisville, PA, 3rd edn, 2013, pp. 175–178.
32 A. Purwanto, F. Ferdiani and R. Damayanti, *Presented in Part at AIP Conference*, Yogyakarta, Indonesia, 2016, DOI: **10.1063/1.4978105**.
33 R. K. Sharma, M. Mishra, S. Sharma and S. Dutta, *J. Coord. Chem.*, 2016, **69**, 1152–1165.
34 J. Kramer, N. E. Dhladhla and K. R. Koch, *Sep. Purif. Technol.*, 2006, **49**, 181–185.
35 G. Perez, E. Erkizia, J. Gaitero, I. Kaltzakorta, I. Jiménez and A. Guerrero, *Mater. Chem. Phys.*, 2015, **165**, 39–48.
36 V. Zeleňák, M. Skřínska, A. Zukal and J. Čejka, *Chem. Eng. J.*, 2018, **348**, 327–337.
37 P. Ramakul, Y. Yanachawakul, N. Leepipatpiboon and N. Sunsandee, *Chem. Eng. J.*, 2012, **193**, 102–111.
38 K. R. Koch, *Coord. Chem. Rev.*, 2001, **216**, 473–488.
39 A. P. Paiva, G. I. Carvalho, M. C. Costa, A. M. da Costa and C. Nogueira, *Solvent Extr. Ion Exch.*, 2013, **32**, 78–94.
40 A. N. Nikoloski and K. L. Ang, *Miner*, 2013, **35**, 369–389.
41 Z. Tu, S. Lu, X. Chang, Z. Li, Z. Hu, L. Zhang and H. Tian, *Microchim. Acta*, 2011, **173**, 231–239.
42 L. Zhou, J. Liu and Z. Liu, *J. Hazard. Mater.*, 2009, **172**, 439–446.
43 P. Chassary, T. Vincent, J. Sanchez-Marcano, L. E. Macaskie and E. Guibal, *Hydrometallurgy*, 2005, **76**, 131–147.
44 A. K. Mosai, L. Chimuka, E. M. Cukrowska, I. A. Kotzé and H. Tutu, *Environ. Dev. Sustain.*, 2020, **23**, 7041–7062.
45 P. R. Zalupski, R. McDowell and G. Dutech, *Solvent Extr. Ion Exch.*, 2014, **32**, 737–748.
46 M. Li, S. Tang, Z. Zhao, X. Meng, F. Gao, S. Jiang, Y. Chen, J. Feng and C. Feng, *Chem. Eng. J.*, 2020, **386**, 123947.
47 W. Wang, X. Liu, X. Wang, L. Zong, Y. Kang and A. Wang, *Front. Chem.*, 2021, **9**, 662482.
48 A. Mavhungu, R. K. Mbaya and M. L. Moropeng, *Int. J. Chem. Eng. Appl.*, 2013, 354–358.
49 C. Defo and R. Kaur, in *Effects of Emerging Chemical Contaminants on Water Resources and Environmental Health*, IGI global, Kenya, 2020, pp. 193–213, DOI: **10.4018/978-1-7998-1871-7**.
50 F. Sevim, O. Lacin, E. F. Ediz and F. Demir, *Environ. Prog. Sustainable Energy*, 2020, **40**, 13471.
51 A. K. Mosai, L. Chimuka, E. M. Cukrowska, I. A. Kotzé and H. Tutu, *Water, Air, Soil Pollut.*, 2019, **230**, 1–17.

52 A. K. Mosai, L. Chimuka, E. M. Cukrowska, I. A. Kotzé and H. Tutu, *Environ. Prog. Sustainable Energy*, 2020, **40**, 13481.
53 Y. Ho and A. Ofomaja, *J. Hazard. Mater.*, 2006, **129**, 137–142.
54 A. N. Ebelegi, N. Ayawei and D. Wankasi, *Open J. Phys. Chem.*, 2020, **10**, 166–182.